Robotica (2009) volume 27, pp. 621–632. © 2008 Cambridge University Press
doi:10.1017/S0263574708005006 Printed in the United Kingdom

Effect of circular arc feet on a control law for a biped

T. Kinugasa†,*, C. Chevallereau‡ and Y. Aoustin‡

†*Okayama University of Science, 1-1, Ridai-cho, Okayama, 700-0005, Japan*
‡*IRCCyN, Ecole Centrale de Nantes, CNRS, Université de Nantes BP 92101, 1, rue de la Noë, 44321 Nantes cedex 3, France*

(Received in Final Form: July 8, 2008. First published online: August 20, 2008)

SUMMARY

The purpose of our research is to study the effects of circular arc feet on the biped walk with a geometric tracking control. The biped studied is planar and is composed of five links and four actuators located at each hip and each knee thus the biped is underactuated in single support phase. A geometric evolution of the biped configuration is controlled, instead of a temporal evolution. The input-output linearization with a PD control law and a feed forward compensation is used for geometric tracking. The controller virtually constrains 4 degrees of freedom (DoF) of the biped, and 1 DoF (the absolute orientation of the biped) remained. The temporal evolution of the remained system with impact events is analyzed using Poincaré map. The map is given by an analytic expression based on the angular momentum about the contact point. The effect of the radii of the circular arc feet on the stability is studied. As a result, the speed of convergence decreases when the radii increases, if the radius is larger than the leg length the cyclic motion is not more stable. Among the stable cyclic motion, larger radius broadens the basin of attraction. Our results agree with those obtained for passive dynamic walking on stability, even if the biped is controlled through the geometric tracking.

KEYWORDS: under-actuated biped; circular arc feet; nonlinear control; stability analysis.

1. Introduction

Over the past several years a considerable amount of studies have been proposed on biped walking. The choice of the type of feet such as contact points, flat feet, and circular arc feet is important, because walking stability is essentially affected by the contact with the ground. Control methods of many traditional humanoids with flat foot are based on zero moment point (ZMP) that remains inside the convex hull of the foot support using the ankle torque. There are lots of successful results, but the gaits seem not to be so natural. On the other hand, for a biped with point contact a geometric tracking method for biped walking using input-output linearization[1–4] produces stable gait that seems quite natural. The idea of the geometric tracking can be seen in the previous studies of Furusho[5] and Kajita.[6] Grizzle, *et al.*[2] proposed the method for a three-link model, only two outputs are controlled, the reference are expressed as a function of the biped state. Zero dynamics with an impact event of the controlled system were analyzed by Poincaré method. The effectiveness of geometric tracking has been verified on a platform called "Rabbit"[4] (Fig. 1 left) with point feet. Westervelt, *et al.*[7] gave some additional results to show the capability for robustness, changing average walking rate, and rejecting a perturbation by "one-step transition control" and "event-based control."

In the domain of passive dynamic walking mechanisms[8], it is shown that a biped with large radius circular arc feet can take easily a lot of steps. The prototype Emu (Fig. 1 right) can be equipped with various arc feet with different radii.[9–11] In the previous walking experiments the biped Emu is excited by gravity or forced oscillation of the length of legs. If the feet radius is 10% of the leg length, the biped could only take few steps[9] excited by the effect of gravity because of the sensitivity to disturbances produced by the cables, the guide to avoid lateral motion and so on. The biped could not walk by the forced oscillation. In the case of a radius which is 97% of the leg length, the biped Emu (Fig. 1 right) can easily take few dozen of steps[10,11] by gravity and leg oscillations. The step number is limited only by the space of our laboratory. The effect of radii of the circular feet was significant for our results, but the change of radius is also accompanied by other difference in physical parameters, thus a direct conclusion on the experimental study is not obvious and a more rigorous study must be done. In fact, the same results are well-known in the field of passive dynamic walking as it is mentioned in Section 2.

The geometric tracking method that was used for the underactuated biped Rabbit can be extended to the case of underactuated biped with circular arc feet. If the biped has the circular arc feet, the analytical stability study given by Chevallereau, *et al.*[4] cannot be applied directly. The contact point between the supporting foot and the ground moves forward during the step in this case. The same difficulty appears also in a flat feet model. For this problem, Djoudi and Chevallereau[12,13] gave a solution to analyze the stability with a chosen evolution of the ZMP.

The purpose of the paper is to show the effects of the circular arc feet for an underactuated planar biped controlled by a geometric tracking method. The effect of the feet shape on the control properties is obviously dependent on the walking strategies. Therefore it is significant to clarify the effect of the feet shape on the geometric tracking even if it is well-known in the passive dynamic walking field.

A model of our biped is composed of five links. Prismatic knee joints are employed to avoid the foot clearance problem which occurs in association with large foot, not actuated

* Corresponding author. E-mail: kinugasa@mech.ous.ac.jp

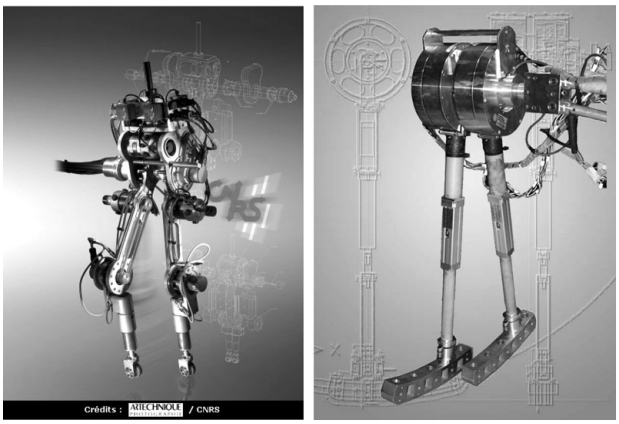

Fig. 1. Biped bipeds, "Rabbit" (left) and "Emu" (right).

ankle and rotational knee joint. A geometric evolution of the biped configuration is controlled, instead of a temporal evolution. The input-output linearization with a PD control law and a feed forward compensation is used for geometric tracking. The temporal evolution is analyzed using Poincaré map. The map is given by an analytic expression based on the angular momentum about the mobile contact point. The effect of the radius of the circular arc feet on stability and the basin of attraction is revealed by analytic calculation. It is compared to the effect of radius of the circular arc feet on passive dynamic walking. Section 2 presents an overview of the previous studies on the circular arc feet. Section 3 gives the biped model. It is composed of a dynamic model and the impact model (instantaneous double support). Section 4 presents the control method. Section 5 gives the stability analysis. Some simulation results are shown and some discussion on the effects of the feet radius are developed in Section 6. Section 7 concludes the paper.

2. Previous Studies on Biped with Circular Arc Feet

Circular arc feet for bipeds are often treated in the field of passive dynamic walking.[8] It is well-known that a passive dynamic walking gives an extremely natural gait. McGeer showed that an eigenvalue of the "speed mode" came to unit when the radius of a circular arc foot approaches the length of legs, and the eigenvalue becomes unit for synthetic wheel which has the foot radius equals to the leg length. The "speed mode" was related to dissipation of energy at the impact.

Wisse, *et al.*[14] showed that larger the feet radius, the larger amount of disturbances are accepted in experiments. The robustness against disturbances is connected to the size of a basin of attraction for walking. Wisse explained in the other paper[15] that "The walker will fall backward if it has not enough velocity to overcome the vertical position. Circular feet smoothen the hip trajectory and thus relax the initial velocity requirement. As a result, the basin of attraction is enlarged." However a decisive study on the effect of circular arc feet on the basin of attraction has yet to be performed. Recently, Wisse, *et al.*[16] presented a stability analysis of passive dynamic walking with flat feet and passive ankles. The effect of the flat feet was analogous to the effect of the circular arc feet for many properties in the sense that ZMP smoothly and monotonically moves forward from heel to toe. However he pointed out the need of validation for a more accurate model of the heel strike transition. Asano and Luo[18] discussed similar effect between the circular arc feet and the flat feet with actuated ankles. Asano and Luo[17] also showed energy effect, step period, walking speed and energy effect of circular feet. However, their result is only showed by numerical simulation. It is important to show the effects through analytic study.

Adamczyk, *et al.*[19] studied the centre of mass (CoM) mechanical work per step with respect to the foot radius for various simple models of biped powered by an instantaneous push-off impulse under the stance foot just before contralateral heel strike.[21] They also showed relationships between foot radius and metabolic costs from measured via respiratory gas exchange. The data are collected through human walking with feet attached to the rigid arc, and they concluded that the most effective walking is obtained when the foot radius equals to 30% of the leg length.

Geometrically speaking, the feet length should be at least twice that of the product of the coxa angle between two legs and the radius of feet.[8] Therefore one might choose the radius as 1/3 of a leg length with an angle 0.3 rad between two legs, in order to make an anthropomorphic biped, as McGeer wrote.

Thus for anthropomorphic models, 1/3 of leg length seems to be desirable in the sense of geometry between step length and feet lengths,[8] "foot clearance problem"[14] and energy costs.[19]

3. The Biped Modeling

A biped presented in Fig. 2 is composed of a torso and two symmetric legs which consist of the prismatic frictionless knees and the circular arc feet. The hips are rotational frictionless joints. We assume that the contact point does not slip and the biped walks in a vertical sagittal plane. The vector $\theta = [l_1, l_2, \theta_1, \theta_2, \theta_3]'$ (" $'$ " means transpose) of configuration variables (see Fig. 2, left) describes the shape of the biped during single support, l_i is the length of leg i, $\theta_i, i = 1, 2$ is the angle between the torso and the leg i, θ_3 is the absolute angle of the supporting leg. The contact point between the biped and the ground is N_1. The lowest point of the swing leg tip is noted N_2. The actuator torques and forces are expressed by a vector $\Gamma = [\Gamma_1, \Gamma_2, \Gamma_3, \Gamma_4]'$. The absolute orientation of the biped θ_3 is not directly actuated. Thus, in a single support (SS), the biped is an underactuated system. The walking gait consists of single support phases separated by impacts, which are instantaneous double supports where a leg exchange takes place.

3.1. Dynamic model for single support phase

The dynamic model can be written as follows:

$$D(\theta)\ddot{\theta} + H(\theta, \dot{\theta}) = B\Gamma, \tag{1}$$

where $D \in \Re^{5\times5}$ is the inertia matrix, the vector $H \in \Re^5$ contains Coriolis, centrifugal, and gravity terms. $B \in \Re^{5\times4}$ defines how the inputs Γ enter the model. Due to the choice of joint coordinates, the matrix B is written as $B = [I_4, O_{4\times1}]'$.

https://doi.org/10.1017/S0263574708005006 Published online by Cambridge University Press

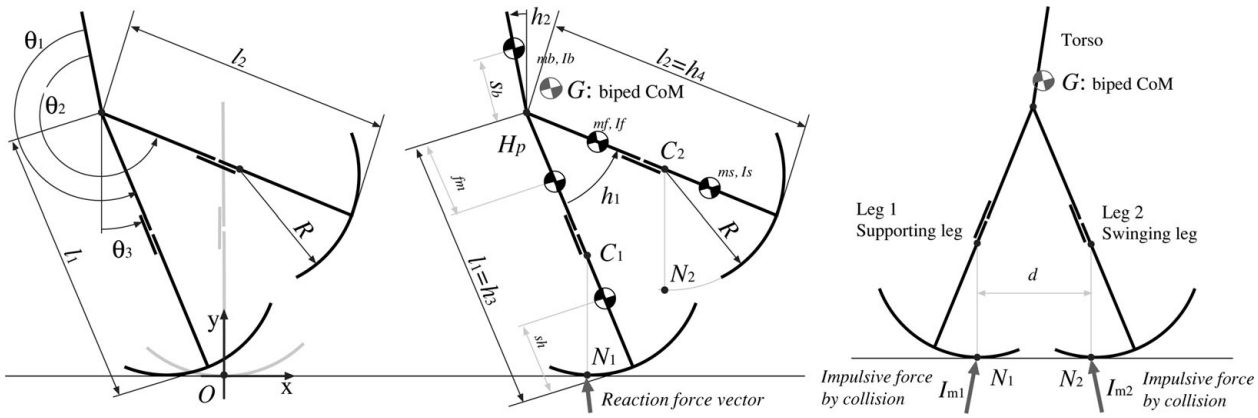

Fig. 2. The biped model. Left: coordinate of the model. Middle: physical parameters. Right: impact model.

3.2. *Impact model*

To derive an impact model, a general dynamic model is written

$$D_e(\theta)\ddot{\theta}_e + H_e(\theta_e, \dot{\theta}) = B_e\Gamma + D_{R_i}(\theta)R_i, \tag{2}$$

where $\theta_e = [\theta', x_H, y_H]'$, and x_H and y_H are the Cartesian coordinates of the hip position H_p shown in Fig. 2 (right), $D_e \in \Re^{7\times7}$ is the inertia matrix, the vector $H_e \in \Re^7$ contains Coriolis, centrifugal, and gravity terms. $R_i = [R_{x_i}, R_{y_i}]'$ is a ground reaction force vector applied at the contact point. $B_e \in \Re^{7\times4}$ and $D_{R_i} \in \Re^{7\times2}$ defines how the inputs Γ and R_i enter the model, i is the number of leg in contact with the ground, $i = 1$, $i = 2$, or $i = 1, 2$.

When the leg i rolls on the ground, the contact with the ground occurs in N_i. If leg i touches the ground and since, we assume that no sliding occurs, the position of N_i is $ON_i = [-R\theta_3, 0]'$, where O is defined such that for the current step, the point contact is in 0 when θ_3 is zero. This position can also be calculated by $ON_i = OH_p + H_pC_i + C_iN_i$ (Fig. 2, middle). Thus, we have

$$\begin{bmatrix} -R\theta_3 \\ 0 \end{bmatrix} = \begin{bmatrix} x_H + (l_i - R)\sin\theta_3 \\ y_H - (l_i - R)\cos\theta_3 - R \end{bmatrix}. \tag{3}$$

Therefore, the following constraint equation is obtained

$$\Psi_i := \begin{bmatrix} x_H + R\theta_3 + (l_i - R)\sin\theta_3 \\ y_H - R - (l_i - R)\cos\theta_3 \end{bmatrix} = 0. \tag{4}$$

Equation (4) is differentiated twice with respect to time, to obtain a constraint on the joint acceleration:

$$D'_{R_i}\ddot{\theta}_e + C_{R_i}(\theta_e, \dot{\theta}_e)\dot{\theta}_e = 0, \tag{5}$$

where $D'_{R_i} = \partial\Psi_i/\partial\theta_e$ and C_{R_i} comes from the derivation.

We assume that the impact is inelastic and instantaneous without sliding. Let $\dot{\theta}_e^-$ and $\dot{\theta}_e^+$ be the angular velocities just before and just after the impact, respectively. Let $I_{m_i} = [I_{mx_i}, I_{my_i}]'$, for $i = 1, 2$ be the vector of magnitudes of the impulsive reaction at the contact point of the stance and the swing leg. During the impact, the previous supporting leg can stay on the ground or take off. If the leg takes off, the velocity of N_1 after the impact is positive. The impulsive ground reaction associated to a leg that stays on the ground must be positive and be in the friction cone. If the supporting leg takes off, the associated impulsive ground reaction is zero. The impact occurs when the leg tip of the swing leg contacts the ground. To take into account the two cases, the following impact equation can be written

$$\begin{cases} D_e(\theta)(\dot{\theta}_e^+ - \dot{\theta}_e^-) = D_R(\theta)I_m \\ D'_R(\theta)\dot{\theta}_e^+ = 0 \end{cases}, \tag{6}$$

where,

$$D_R(\theta) = \begin{cases} D_{R_2}(\theta), & \dot{y}_{N_1}^+ > 0 \\ D_{R_{12}}(\theta), & I_{my_1} > 0,\ I_{my_2} > 0, \end{cases}$$

$$I_m = \begin{cases} I_{m_2}, & \dot{y}_{N_1}^+ > 0 \\ I_{m_{12}}, & I_{my_1} > 0,\ I_{my_2} > 0, \end{cases}$$

$$D_{R_{12}}(\theta) = \begin{bmatrix} D_{R_1}(\theta) & 0 \\ 0 & D_{R_2}(\theta) \end{bmatrix}, \quad I_{m_{12}} = \begin{bmatrix} I_{m_1} \\ I_{m_2} \end{bmatrix}.$$

From Eq. (6), we obtain

$$\dot{\theta}_e^+ = \left(I_{7\times7} - D_e^{-1}D_R\left(D'_R D_e^{-1} D_R\right)^{-1} D'_R\right)\cdot\dot{\theta}_e^-. \tag{7}$$

Before and after the impact, the biped is in contact with the ground on at least one leg, thus x_H, y_H can be calculated as function of θ, and $\dot{x}_H$, $\dot{y}_H$ can be calculated as function of $\dot{\theta}$. Equation (7) can be transformed into an equation of θ, $\dot{\theta}$ only.

$$\dot{\theta}^+ = \Delta(\theta)\dot{\theta}^-, \tag{8}$$

where $\Delta(\theta) \in \Re^{5\times5}$ is the impact matrix. This matrix depends on the foot radius R. In the gait studied, the legs swap their roles from one step to the next, thus since the biped is symmetric, the dynamic model is derived only for the support on leg 1. And the leg exchange is taken into account just after the impact. The state of the biped to begin the next step is

$$\theta_i = T_{LS}\theta_f, \quad \dot{\theta}_i = T_{LS}\dot{\theta}^+, \ \dot{\theta}^+ = \Delta(\theta_f)\dot{\theta}_f, \tag{9}$$

https://doi.org/10.1017/S0263574708005006 Published online by Cambridge University Press

where $T_{LS} \in \Re^{5\times5}$ is the permutation matrix describing the leg exchange, the indexes $_{i,f}$ denoted the initial and final states of the biped for one step.

4. Control Law

Since the studied biped is underactuated, and since some good results have been obtained for the control of underactuated biped with point contact,[4,7] our strategy for walking is to control four variables, such that they track the reference defined with respect to the monotonic variable θ_3. The four variables that are controlled are grouped in vector $h = [h_1, h_2, h_3, h_4]' = [\theta_2 - \theta_1, \theta_3 - \theta_1 + \pi, l_1, l_2]'$, composed of the angle between two legs, the absolute angle of the torso, and the leg lengths, (shown in Fig. 2, middle). This vector h, plus θ_3 defines the configuration of the biped. The relation with vector θ is the following:

$$\theta = \begin{bmatrix} h_3 \\ h_4 \\ -h_2 + \theta_3 \\ h_1 - h_2 + \theta_3 \\ \theta_3 \end{bmatrix} = \begin{bmatrix} 0 & 0 & 1 & 0 \\ 0 & 0 & 0 & 1 \\ 0 & -1 & 0 & 0 \\ 1 & -1 & 0 & 0 \\ 0 & 0 & 0 & 0 \end{bmatrix} h + \begin{bmatrix} 0 \\ 0 \\ 1 \\ 1 \\ 1 \end{bmatrix} \theta_3 \tag{10}$$

$$\theta = \frac{\partial\theta}{\partial h} h + \frac{\partial\theta}{\partial\theta_3}\theta_3, \tag{11}$$

where $\frac{\partial\theta}{\partial h}$ and $\frac{\partial\theta}{\partial\theta_3}$ are the constant matrices given in (10). Thus we also have

$$\ddot{\theta} = \frac{\partial\theta}{\partial h}\ddot{h} + \frac{\partial\theta}{\partial\theta_3}\ddot{\theta}_3. \tag{12}$$

The control law is based on a computed torque control law and is such that the behavior of the controlled variables are

$$\ddot{h} = \ddot{h}^d - K_p(h - h^d) - K_d(\dot{h} - \dot{h}^d). \tag{13}$$

But the reference to follow is a function of the variable θ_3 thus the reference is

$$h^d = h^d(\theta_3) \tag{14}$$

$$\dot{h}^d = \frac{dh^d}{d\theta_3}(\theta_3)\dot{\theta}_3 \tag{15}$$

$$\ddot{h}^d = \frac{dh^d}{d\theta_3}(\theta_3)\ddot{\theta}_3 + \frac{d^2h^d}{d\theta_3^2}(\theta_3)\dot{\theta}_3^2. \tag{16}$$

Thus the desired behavior in a closed loop is given by

$$\ddot{h} = \frac{dh^d}{d\theta_3}(\theta_3)\ddot{\theta}_3 + \frac{d^2h^d}{d\theta_3^2}(\theta_3)\dot{\theta}_3^2 - K_p(h - h^d(\theta_3)) - K_d(\dot{h} - \frac{dh^d}{d\theta_3}(\theta_3)\dot{\theta}_3). \tag{17}$$

This expression is denoted by

$$\ddot{h} = \frac{dh^d}{d\theta_3}(\theta_3)\ddot{\theta}_3 + v(\theta, \dot{\theta}). \tag{18}$$

The dynamic model (1) can be expressed as a function of $\ddot{h}$ and $\ddot{\theta}_3$ using (12)

$$D(\theta)\left(\frac{\partial\theta}{\partial h}\ddot{h} + \frac{\partial\theta}{\partial\theta_3}\ddot{\theta}_3\right) + H(\theta, \dot{\theta}) = B\Gamma. \tag{19}$$

The torques will be calculated in order to have in closed loop the behavior given in (18), thus the torques must satisfy

$$D(\theta)\left(\left(\frac{\partial\theta}{\partial h}\frac{dh^d}{d\theta_3}(\theta_3) + \frac{\partial\theta}{\partial\theta_3}\right)\ddot{\theta}_3 + \frac{\partial\theta}{\partial h}v(\theta, \dot{\theta})\right) + H(\theta, \dot{\theta}) = B\Gamma. \tag{20}$$

Since the biped is underactuated, not all motions are possible and based on the expression of matrix B, the admissible acceleration $\ddot{\theta}_3$ can be deduced. The dynamic model is decomposed into two submodels. The first submodel is composed of the first four lines and allows to calculate the torque. The second sub model is composed of the fifth line and allows to calculate $\ddot{\theta}_3$. This subsystem gives

$$\ddot{\theta}_3 = \frac{-D_5(\theta)\frac{\partial\theta}{\partial h}v(\theta, \dot{\theta}) - H_5(\theta, \dot{\theta})}{D_5(\theta)\left(\frac{\partial\theta}{\partial h}\frac{dh^d}{d\theta_3}(\theta_3) + \frac{\partial\theta}{\partial\theta_3}\right)}, \tag{21}$$

where the index 5 refers to the 5th line of matrix D and vector H.

Finally, the control law is obtained

$$\Gamma = D_{1,4}(\theta)\left(\left(\frac{\partial\theta}{\partial h}\frac{dh^d}{d\theta_3}(\theta_3) + \frac{\partial\theta}{\partial\theta_3}\right)\ddot{\theta}_3 + \frac{\partial\theta}{\partial h}v(\theta, \dot{\theta})\right) + H_{1,4}(\theta, \dot{\theta}), \tag{22}$$

where the indexes 1, 4 refer to the first four lines of matrix D and vector H.

5. Stability Analysis

With the control, the output vector h converges to the reference path $h^d(\theta_3)$, and if the reference function is such that the impact condition is satisfied, the output is zero step after step for convenient choice of the control gains K_p, K_d.[20]

5.1. Reference path

Since the initial and final configurations for a single support are double support configurations, when h^d is given, θ_3 can be deduced from geometrical relations. Thus the initial and final values of θ_3 on one step are known and denoted by θ_{3i} and θ_{3f}. Since the condition of the impact is a geometrical condition, if the control law has converged and if θ_3 has a monotonic evolution, the configuration at the impact is the desired one. The reference function is designed such that the

https://doi.org/10.1017/S0263574708005006 Published online by Cambridge University Press

impact condition is satisfied. According to equations (8), (9), and (11), the reference path must be such that

$$\theta(\theta_{3i}) = T_{LS}\theta(\theta_{3f}). \tag{23}$$

$$\left(\frac{\partial\theta}{\partial h}\frac{\partial h^d}{\partial\theta_3}(\theta_{3i}) + \frac{\partial\theta}{\partial\theta_3}\right)\dot{\theta}_{3i} = T_{LS}\Delta(\theta_{3f})\left(\frac{\partial\theta}{\partial h}\frac{\partial h^d}{\partial\theta_3}(\theta_{3f}) + \frac{\partial\theta}{\partial\theta_3}\right)\dot{\theta}_{3f}. \tag{24}$$

Equality (24) is composed of five scalar equations, thus $\frac{\partial h^d}{\partial\theta_3}(\theta_{3i})$ and $\frac{\dot{\theta}_{3i}}{\dot{\theta}_{3f}}$ can be calculated as function of $\frac{\partial h^d}{\partial\theta_3}(\theta_{3f})$. The ratio of velocities is denoted by $\delta_{\dot{\theta}_3}$:

$$\delta_{\dot{\theta}_3} = \frac{\dot{\theta}_{3i}}{\dot{\theta}_{3f}}. \tag{25}$$

5.2. Principle of the stability analysis

With the control law, the output vector h converges to the reference path $h^d(\theta_3)$. In the following section we assume that $h = h^d(\theta_3)$, that is, the system tracks the reference path. The 5 DoF of the biped can be reduced to 1 DoF of a virtual equivalent pendulum under the condition, and we will hence analyze stability of the pendulum instead of the original biped.

This condition does not mean that the biped motion is cyclic with respect to time since the temporal evolution of θ_3 is the result of integration of Eq. (21), and thus depends on the reference path $h^d(\theta_3)$. For an SS phase, θ_3 must evolve monotonically from θ_{3i} to θ_{3f}. The temporal evolution of the biped during an SS phase is completely defined by the velocity $\dot{\theta}_3$ for one particular value θ_3. The stability analysis is based on the Poincaré return map, and this return map will be built just before the impact, when the biped is in the configuration $h^d(\theta_{3f}), \theta_{3f}$. The variable that is effective to study the convergence to a cyclic motion is $\dot{\theta}_{3f}$. Since the angular momentum is proportional to $\dot{\theta}_{3f}$, the angular momentum (or its square value) can also be used in the stability analysis.

5.3. SS phase

According the Newton–Euler second law, as the gravity is the only external force that produces a torque around N_1, the equilibrium of the biped in rotation around the mobile contact point N_1 gives

$$\dot{\sigma}_{N_1} + MV_{N_1} \times V_G = \vec{N_1G} \times M\vec{g}, \tag{26}$$

where V_{N_1} and V_G are the velocities at the points $N_1 = [-R\theta_3, 0]'$ and the center of mass, $G = [x_G, y_G]'$, M is the total mass of the biped, the gravity vector is $\vec{g} = [0, -g]'$, and σ_{N_1} is the angular momentum about N_1. The general expression of σ_{N_1} is

$$\sigma_{N_1} = \sum_i m_i \ \vec{N_1G_i} \times V_{Gi} + \sum_i I_i w_i, \tag{27}$$

where G_i is the center of mass for the link i, m_i and I_i are the mass and the inertia of link i, w_i is the angular velocity of link i, and V_{Gi} is the linear velocity of G_i. This quantity is linear with respect to the joint velocity component and can be written

$$\sigma_{N_1} = S(\theta)\dot{\theta}. \tag{28}$$

We assume that the biped follows reference path thus we have

$$\theta = \frac{\partial\theta}{\partial h}h^d(\theta_3) + \frac{\partial\theta}{\partial\theta_3}\theta_3. \tag{29}$$

$$\dot{\theta} = \frac{\partial\theta}{\partial h}\frac{\partial h^d}{\partial\theta_3}(\theta_3)\dot{\theta}_3 + \frac{\partial\theta}{\partial\theta_3}\dot{\theta}_3. \tag{30}$$

Thus the angular momentum σ_{N_1} (28) is rewritten

$$\sigma_{N_1} = S(\theta)\left(\frac{\partial\theta}{\partial h}\frac{\partial h^d}{\partial\theta_3}(\theta_3) + \frac{\partial\theta}{\partial\theta_3}\right)\dot{\theta}_3 = I_{\theta_3}(\theta_3)\dot{\theta}_3. \tag{31}$$

Equation (26) can be developed using the expression of $\vec{N_1G}$, V_G, V_{N_1} as

$$\dot{\sigma}_{N_1} = -Mg(x_G(\theta_3) + R\theta_3) + MR\frac{dy_G(\theta_3)}{d\theta_3}\dot{\theta}_3^2. \tag{32}$$

Equation (31) is combined to Eq. (32) to express the derivative of σ_{N_1} with respect to θ_3, under the assumption that θ_3 is monotonic:

$$\frac{d\sigma_{N_1}}{d\theta_3} = -Mg(x_G + R\theta_3)\frac{I_{\theta_3}}{\sigma_{N_1}} + MR\frac{dy_G}{d\theta_3}\frac{\sigma_{N_1}}{I_{\theta_3}}. \tag{33}$$

A new variable $\xi = \sigma_{N_1}^2/2$ is introduced, to transform Eq. (33) into an equation that can be integrated analytically:

$$\begin{aligned}\frac{d\xi}{d\theta_3} &= \kappa_1(\theta_3) + 2\kappa_2(\theta_3)\xi,\\ \kappa_1(\theta_3) &= -Mg(x_G + R\theta_3)I_{\theta_3},\\ \kappa_2(\theta_3) &= \frac{MR}{I_{\theta_3}}\left(\frac{\partial y_G(\theta)}{\partial\theta}\right)'\frac{d\theta^d}{d\theta_3}.\end{aligned} \tag{34}$$

Equation (34) is a first-order ordinary differential equation linear in ξ. Therefore, a general solution can be obtained, for a step that begins with θ_{3i} as an initial value:

$$\xi(\theta_3) = \delta_{SS}^2(\theta_3)\xi(\theta_{3i}) + V(\theta_3), \tag{35}$$

$$\delta_{SS}(\theta_3) = \exp\left(\int_{\theta_{3i}}^{\theta_3}\kappa_2(\tau_2)d\tau_2\right), \tag{36}$$

$$V(\theta_3) = \int_{\theta_{3i}}^{\theta_3}\exp\left(\int_{\tau_1}^{\theta_3}2\kappa_2(\tau_2)d\tau_2\right)\kappa_1(\tau_1)\,d\tau_1. \tag{37}$$

ξ and V are a pseudo-kinetic and a pseudo-potential energies of the virtual equivalent pendulum, respectively.

https://doi.org/10.1017/S0263574708005006 Published online by Cambridge University Press

As a consequence if $\dot{\theta}_{3i}$ is known $\dot{\theta}_3$ can be deduced for the current step as a function of V and δ_{SS} without integration of (26). To be able to deduce from this equation the evolution of ξ (and in consequence of σ_{N_1} and $\dot{\theta}_3$) step after step and the evolution of ξ at the impact must be taken into account. In the following section, the index k will be added to denote the number of the current step.

5.4. Impact phase

Let us consider the impact between steps k and $k+1$. Using (31), ξ at the end of step k is

$$\xi_k(\theta_{3f}) = \frac{1}{2}(I_{\theta_{3f}}(\theta_{3f})\dot{\theta}_{3f,k})^2 \tag{38}$$

and ξ at the beginning of the step $k+1$ is

$$\xi_{k+1}(\theta_{3i}) = \frac{1}{2}(I_{\theta_{3i}}(\theta_{3i})\dot{\theta}_{3i,k+1})^2. \tag{39}$$

Using (25), and defining δ_I by

$$\delta_I = I_{\theta_3}(\theta_{3i})/I_{\theta_3}(\theta_{3f}), \tag{40}$$

we obtain

$$\xi_{k+1}(\theta_{3i}) = \delta_I^2\delta_{\dot{\theta}_3}^2\xi_k(\theta_{3f}). \tag{41}$$

5.5. Poincaré map

Combining (35) and (41), the final value of ξ from the kth step to the $(k+1)$th step is as follows:

$$\xi_{k+1}(\theta_{3f}) = \delta^2(\theta_{3f})\xi_k(\theta_{3f}) + V(\theta_{3f}), \tag{42}$$

$$\delta(\theta_{3f}) = \delta_{SS}(\theta_{3f})\delta_I\delta_{\dot{\theta}_3}, \tag{43}$$

where θ_{3f} is the value of θ_3 just before the impact. This equation describes the Poincaré map.

If a cyclic motion exists, then $\xi_{k+1}(\theta_{3f})$ corresponds to $\xi_k(\theta_{3f})$. Thus, a fixed point $\xi_c(\theta_{3f})$ is given using (42) as follows:

$$\xi_c(\theta_{3f}) = \frac{V(\theta_{3f})}{1-\delta^2(\theta_{3f})}. \tag{44}$$

Since $\xi_c(\theta_{3f})$ is positive, $V(\theta_{3f})$ and $1-\delta^2(\theta_{3f})$ must have the same sign. The following cases can occur:

Case 1: From (42), the fixed point is stable, if $\delta^2(\theta_{3f}) < 1$. Therefore, if $\delta^2(\theta_{3f}) < 1$ and $V(\theta_{3f}) > 0$, then an asymptotically stable cyclic motion exists.

Case 2: If $\delta^2(\theta_{3f}) = 1$ and $V(\theta_{3f}) = 0$, from (42), $\xi_{k+1}(\theta_{3f}) = \xi_k(\theta_{3f})$, namely, all motions are cyclic.

Case 3: From (42), the fixed point is unstable, if $\delta^2(\theta_{3f}) > 1$. Therefore, if $\delta^2(\theta_{3f}) > 1$ and $V(\theta_{3f}) < 0$, then an unstable cyclic motion exists.

Case 4: $V(\theta_{3f})(1-\delta^2(\theta_{3f})) < 0$, no cyclic motion exists.

Since by definition $\xi \geq 0$, from Eq. (35) for the complete step, ξ_c must satisfy the following inequality:

$$\xi_c(\theta_{3f}) \geq \xi_{\min} = \max_{\theta_3} \frac{-V(\theta_3)}{\delta^2(\theta_3)} \tag{45}$$

to have $\xi(\theta_3) > 0$ for θ_3 between θ_{3i} and θ_{3f}.

Since a product of the two variables $(\delta_I \cdot \delta_{\dot{\theta}_3})$ is the ratio of momentum σ_{N_1} at the contact point N_1 before and after the impact, the speed of convergence is mainly associated with this ratio (This point will be detailed in the following sections), and connected to the distance between the contact points and velocity of the mass center before the impact.[22]

The contact point before the impact, at the end of the single support phase, is denoted N_1, the contact point after the impact, at the beginning of the next single support phase, is denoted N_2. Using equilibrium relation it is possible to compute the change of angular momentum around the contact point at impact as function of the value of the radii.

The distance d between the N_1 and N_2 is (see Fig. 2)

$$N_1N_2 = d = 2(l-R)\sin(h_1/2). \tag{46}$$

The angular momentum before the impact denoted by $\sigma_{N_1}^-$ is calculated around N_1 and can also be calculated around N_2, it is then denoted by $\sigma_{N_2}^-$, the angular momentum transfer gives

$$\sigma_{N_2}^- = \sigma_{N_1}^- - M \cdot d \cdot \dot{y}_G^-. \tag{47}$$

At the impact, considering the vertical component I_{my_1} of the impulsive ground reaction I_{m_1} in the point N_1, the equilibrium in rotation around N_2 gives

$$\sigma_{N_2}^+ = \sigma_{N_2}^- - d \cdot I_{my_1}, \tag{48}$$

where I_{my_1} is the vertical component of the impulsive ground reaction I_{m_1} applied by the ground in N_1. The vertical equilibrium of the biped at the impact is

$$I_{my_1} + I_{my_2} = M(\dot{y}_G^+ - \dot{y}_G^-), \tag{49}$$

where I_{my_1} and I_{my_2} are the vertical components of the impulsive ground reactions I_{m_1} and I_{m_2} respectively in the points N_1 and N_2. The impact are such that the two legs stay on the ground, thus $I_{my_1} > 0$ and $I_{my_2} > 0$ and we have

$$0 < I_{my_1} < M(\dot{y}_G^+ - \dot{y}_G^-). \tag{50}$$

As a consequence, combining (47), (48), and (50), we have

$$\sigma_{N_1}^- - M \cdot d \cdot \dot{y}_G^+ < \sigma_{N_2}^+ < \sigma_{N_1}^- - M \cdot d \cdot \dot{y}_G^-, \text{ if } d > 0, \tag{51}$$

$$\sigma_{N_2}^+ = \sigma_{N_1}^-, \qquad \text{if } d = 0, \tag{52}$$

$$\sigma_{N_1}^- - M \cdot d \cdot \dot{y}_G^- < \sigma_{N_2}^+ < \sigma_{N_1}^- - M \cdot d \cdot \dot{y}_G^+, \text{ if } d < 0. \tag{53}$$

When $I_{\theta_3} > 0$ (we will show in Fig. 7) and $\dot{\theta}_3 < 0$ (see Fig. 3), $\sigma_{N_1}^- < 0$. Considering (25), (31), and (40), the ratio $\delta_I\delta_{\dot{\theta}_3}$ is

https://doi.org/10.1017/S0263574708005006 Published online by Cambridge University Press

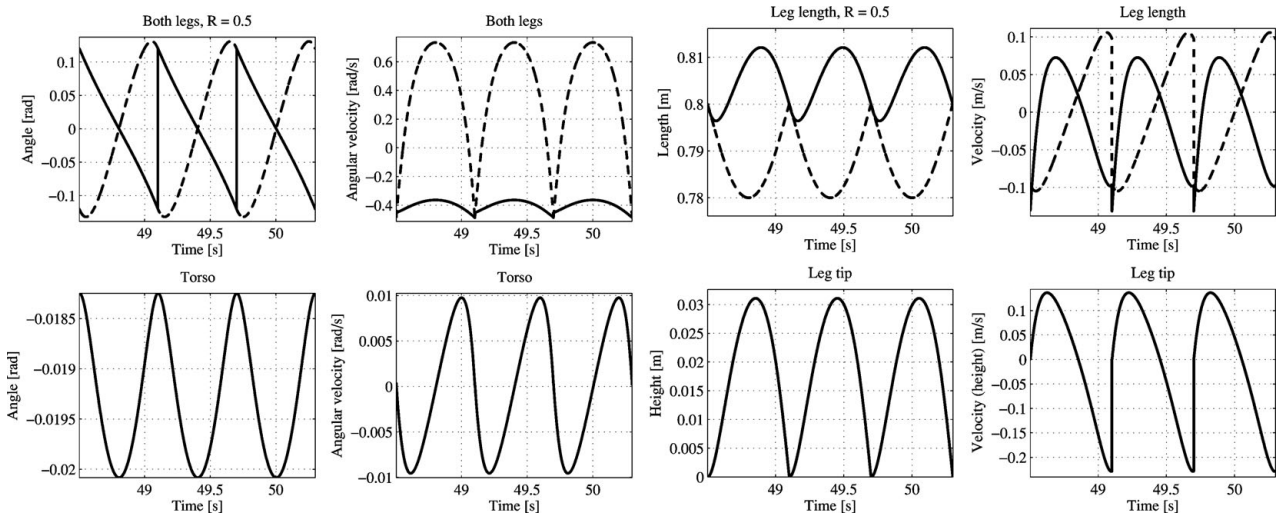

Fig. 3. Time responses at the cyclic motion with $R = 0.5$ m of the angle of both the legs, the torso, the length of legs, and the leg tip. The reference paths are very well tracked.

bounded

$$1 - M \cdot d \cdot \frac{\dot{y}_G^-}{\sigma_{N_1}^-} < \delta_I \delta_{\dot{\theta}_3} < 1 - M \cdot d \cdot \frac{\dot{y}_G^+}{\sigma_{N_1}^-}, \ (d > 0), \quad (54)$$

$$\delta_I \delta_{\dot{\theta}_3} = 1, \qquad (d = 0), \quad (55)$$

$$1 - M \cdot d \cdot \frac{\dot{y}_G^+}{\sigma_{N_1}^-} < \delta_I \delta_{\dot{\theta}_3} < 1 - M \cdot d \cdot \frac{\dot{y}_G^-}{\sigma_{N_1}^-}, \ (d < 0) \quad (56)$$

6. Simulation

In simulations, the physical parameters of the biped shown in Fig. 2 are used (see Table I). The gains of the control law are chosen so that the tracking errors can be smaller than 10^{-4} for all walking gaits

$$\begin{cases} K_p = \text{diag}([10^5, 10^4, 10^5, 5 \times 10^4]) \\ K_d = \text{diag}([5 \times 10^2, 5 \times 10^2, 10^3, 5 \times 10^2]). \end{cases} \quad (57)$$

6.1. Design of reference path

The reference path h^d is defined by a fourth-order polynomial function such that

$$h_d(\theta_3) = a\left[1, \ \theta_3^1, \ \theta_3^2, \ \theta_3^3, \ \theta_3^4\right]', \quad (58)$$

where $a \in \Re^{4\times 5}$ is a coefficient matrix for the reference h_d. An intermediate position of SS phase, positions and derivative with respect to θ just before the impact are given in order to calculate the coefficients of the reference paths (see Fig. 4). Position and derivative with respect to θ after the impact are calculated by equations (23) and (24) .

Table I. Physical parameters for the dynamic model.

m_s	1 kg	I_s	0.05 kg m^2	s_h	0.4 m	l_1	0.8–0.85 m
m_f	1 kg	I_f	0.05 kg m^2	f_m	0.2 m	l_2	0.75–0.8 m
m_b	15 kg	I_b	3 kg m^2	s_b	0.1 m	R	0–1.0 m

Walking is dependent not only on the radii of the feet but also on the reference path of the length of the legs. The foot radius reduces the velocity of the CoM before the impact. The reference paths of the legs are chosen to smoothen the vertical variation of the CoM. However the references of the legs are affected by the impact, and the choice of the reference paths is limited accordingly. The radius mainly smoothens the vertical CoM motion.

The initial and the final length for both the legs are chosen as the same value. The final velocity for the biped are arbitrary fixed. The intermediate configuration for the legs is chosen such that the swing leg length decreases 0.02 m and the stance leg length increases 0.01 m during the step to avoid that the swing leg tip touches the ground and the length of the legs is 0.8 m at the impact. Therefore the top position of the CoM is almost the same for each foot radius as shown in Fig. 5. For one value R, we choose the angle of the torso at the impact arbitrary. The angle of the torso at the intermediate configuration is equal to 110% of the value of the torso angle

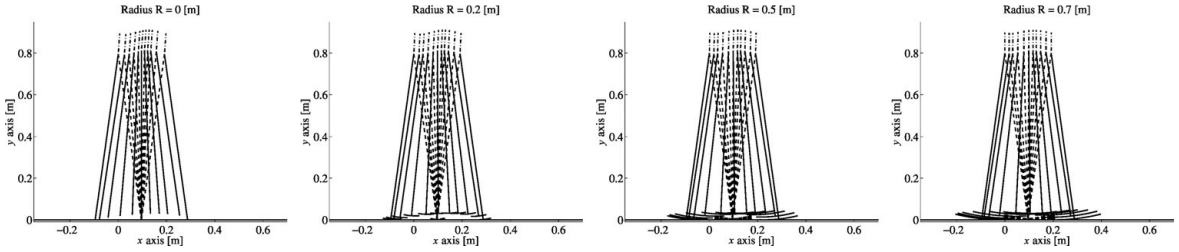

Fig. 4. The stick diagrams of walking. The foot radii $R = 0$ m, 0.2 m, 0.5 m, and 0.7 m from the left figure.

https://doi.org/10.1017/S0263574708005006 Published online by Cambridge University Press

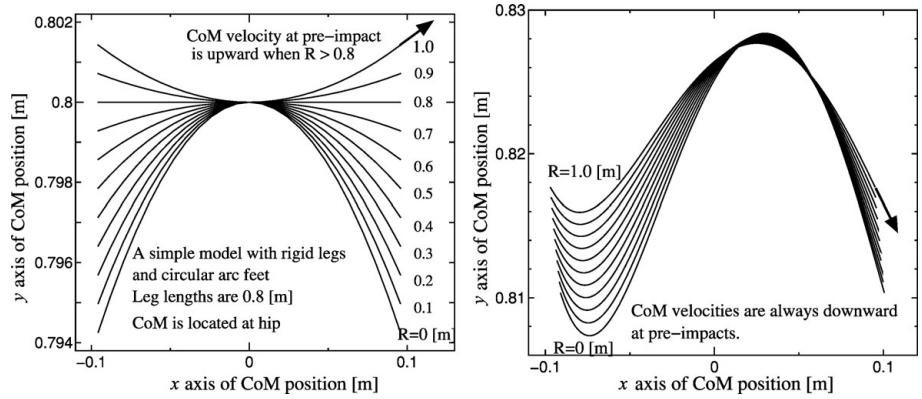

Fig. 5. CoM positions with respect to R. Left: the case of our biped shown in Fig. 2. Tangent vectors of right ends of lines are expressing a post-impact velocity of CoM. Right: the case of a simple model with rigid legs and circular arc feet. CoM is located at hip position. When R > 0.8 m, CoM velocities are upward. It gives a contradiction at the impact or there would be a flight phase.

at the impact. The corresponding value $\xi_c(\theta_{3f})$ is deduced. For example, the coefficient matrix in Eq. (58) for $R = 0.5$ is obtained as follows:

$$a|_{R=0.5} = \begin{bmatrix} 0 & -3.02 & -0.158 & 70.8 & 10.9 \\ -0.0201 & 0.0002 & 0.255 & -0.0106 & -8.89 \\ 0.810 & -0.122 & -1.58 & 8.50 & 61.2 \\ 0.780 & -0.0037 & 1.91 & 0.254 & -36.5 \end{bmatrix} \tag{59}$$

Then from this reference motion we deduced the reference motion for the other value of radius R. The angle of the torso at the impact $h_2(\theta_{3f})$ is adjusted such that the cyclic motions for all the foot radii R have the same value $\xi_c(\theta_{3f})$ as shown in Table II.

Figure 4 shows examples of stick diagrams of walking for one step with the foot radii $R = 0$ m, 0.2 m, 0.5 m, and 0.7 m and the step angle = 0.24 rad. A cyclic motion for $R = 0.5$ m is given in Fig. 3. CoM positions with respect to R are shown in Fig. 5. Tangent vectors of right ends of lines are expressing a post-impact velocity of CoM. The variation of CoM velocities at the impact are presented in Fig. 6.

Energy excitation for continuous walking with smaller feet radius is mainly done by the asymmetric mass distribution due to the torso forward inclination. Leg swing also provides a way of putting energy. For small feet radii, the energy for walking is produced by the weight of the torso that is inclined forward. For larger feet radii, the energy for walking is produced by the motion of the swing leg.

Since the impact equation changes, the initial configuration and velocity are changed accordingly. During the impact, for the chosen reference path, the two legs stay on the ground.

Table II. Torso angles. The angles are chosen such that cyclic motions have the same value $\xi_c(\theta_{3f}) = \xi(-0.12) = 16.27$.

Foot radius [m]	0	0.1	0.2	0.3	
Angle of torso [rad]	−0.060	−0.051	−0.043	−0.034	
Foot radius [m]	0.4	0.5	0.6	0.7	0.8
Angle of torso [rad]	−0.026	−0.018	−0.011	−0.004	0.002

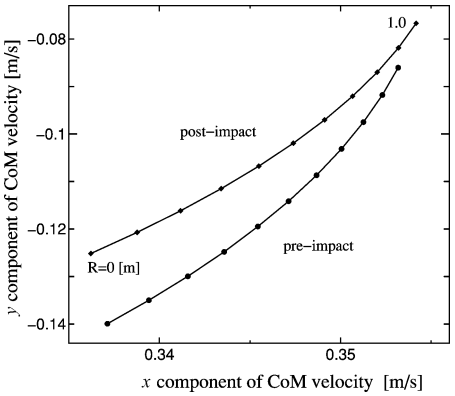

Fig. 6. CoM velocities at the impact with respect to R. The point corresponds to different value of R from 0 to 1, the abscissa of the point gives the horizontal velocity $\dot{x}_G$ respectively before and after the impact, the ordinates gives the vertical velocity $\dot{y}_G$ respectively before and after the impact. The vertical velocities before the impact are always directed downward.

6.2. *Stability analysis in simulation*

The variables in the analytic solution (35) are shown in Fig. 7 with respect to the monotonic variable θ_3 for various values of the foot radius R. It should be noted that the monotonic variable is evolving from a positive value to a negative value, $\theta_3 : 0.12 \text{ rad} \rightarrow -0.12$ rad. In Fig. 7, $\xi_c(\theta)$ is given for all the cyclic motions. It can be observed that $\xi_c(\theta_{3f}) = \xi(-0.12) = 16.27$. The figure of $\delta^2_{SS}(\theta_3)$ is given by Eq. (36). The convergence of Poincaré map, as shown in Eq. (43), is function of $\delta^2_{SS}(\theta_{3f}) = \delta^2_{SS}(-0.12)$. However the values of $\delta^2_{SS}(-0.12)$ are very close to unit thus the convergence of Poincaré map is essentially defined by the impact map : $\delta(\theta_{3f}) \approx \delta_I \delta_{\dot{\theta}_3}$. The second figure from the left of Fig. 7 represents the evolution of V defined by Eq. (37). These functions are essentially affected by the evolution ξ. The third figure of Fig. 7 shows the term I_{θ_3} given by Eq. (31), I_{θ_3} is always positive and has not large variation.

This first study concerns reference path with an interlink angle at the impact equals to 0.24 rad. For this value, the evolution of $\delta^2_{SS}(\theta_{3f})$, δ_I, $\delta_{\dot{\theta}_3}$, and $\delta(\theta_{3f})$ are given in solid line in Fig. 8, as a function of R. The cyclic motion is stable for $R < 0.8$ m.

https://doi.org/10.1017/S0263574708005006 Published online by Cambridge University Press

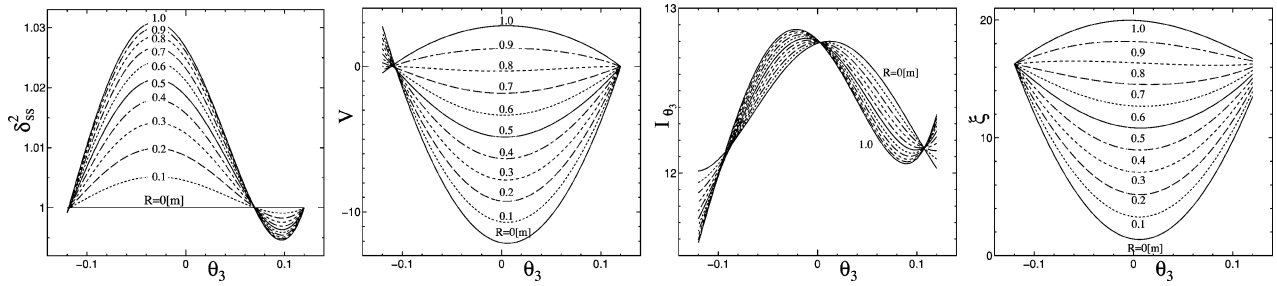

Fig. 7. Analytic solutions for SS phase. The figures are δ^2_{SS} by Eq. (36), V by Eq. (37), the function I_{θ_3} by Eq.(31), and ξ by Eq. (35) from the left. θ_3 evolves from positive (0.12) to negative (-0.12).

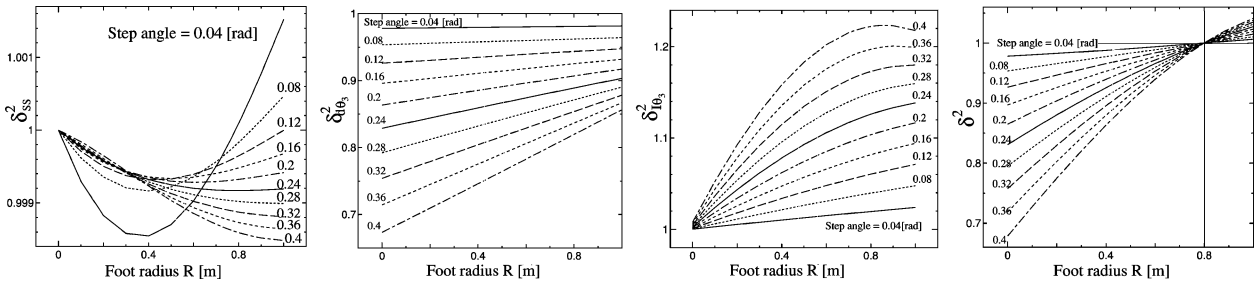

Fig. 8. Slope of the Poincaré return map. Step angle which means angles between two legs at the impact varies from 0.04 rad to 0.40 rad. The figures show δ^2_{SS}, $\delta^2_{\dot\theta_3}$, $\delta^2_{I_{\theta_3}}$ and δ^2 with respect to the foot radii $R = 0 \sim 1.0$ m from the left figure. $R = 0.8$ m means that the radius is the same as the leg length at the impact for the analytic solution. For $R > 0.8$ m, the cyclic motion is not stable.

In order to determine if the radius $R = 0.8$ m is a limit of stability only for one specific reference path or if this limit is more physical, different kinds of reference motion are considered in the following. Only the interlink angle $h_1(\theta_{3f})$ at the impact is changed. For different values of h_1 and radii R, the coefficient involves in the convergence condition are drawn in Fig. 8.

$\delta_{\dot\theta_3}$ and δ_I increase when R increases and $h_1(\theta_{3f})$ decreases from Fig. 8. δ^2 also increases at the same time. The term δ^2 comes to unit when $R = 0.8$ m which means that R has the same values as the length of legs at the impact.

Remark 1 *We confirmed in other simulations that variations of the torso angle had small influences on δ_I and $\delta_{\dot\theta_3}$ although it essentially affects ξ. The variables V, δ_{SS}, I_{θ_3}, and ξ in the analytic solution for SS phase change for the torso angle. However the variation of δ_{SS} is smaller than the variations of δ_I and $\delta_{\dot\theta_3}$ with respect to the foot radii.* △

Figure 9 presents the stability property with respect to the foot radii. Two black rigid lines show V and $\delta^2 - 1$. V and $\delta^2 - 1$ have opposite sign thus a cyclic motion may exist such that (45) is satisfied for any value of radii R. For $R < 0.8$ m, the motion is stable. For $R > 0.8$ m, the motion is unstable. For $R = 0.8$ m, the motion is neutral, in this case any value ξ_c produces cyclic motions.

Case corresponding to a radius larger than the length of each leg, ($R > 0.8$ m) can be studied if we consider that the motions of feet are not in the same sagittal plane to avoid collisions. In the leg exchange, at the impact, the contact point moves back but the contact point has a large forward progression during the single support phase, the biped goes forward.

The gradient δ^2 (Eq. (43)) of Poincaré map (Eq. (42)) depends on the SS phase (δ_{SS}) and the impact phase ($\delta_I \cdot \delta_{\dot\theta_3}$). δ_{SS} was close to unit at the impact. Since $\dot y_G^- < \dot y_G^+ < 0$ (see Fig. 6), we obtain that the foot radius R and the sign of d defined the position of the ratio $\delta_I \delta_{\dot\theta_3}$ with respect to 1 from Eq. (54) to Eq. (56).

- if $R < l$, $d > 0$, and $\delta_I \delta_{\dot\theta_3} < 1$
- if $R = l$, $d = 0$, and $\delta_I \delta_{\dot\theta_3} = 1$
- if $R > l$, $d < 0$, and $\delta_I \delta_{\dot\theta_3} > 1$

The property of the gradient δ^2 agrees with "speed mode" of passive dynamic walking obtained by McGeer.[8] Wisse[16]

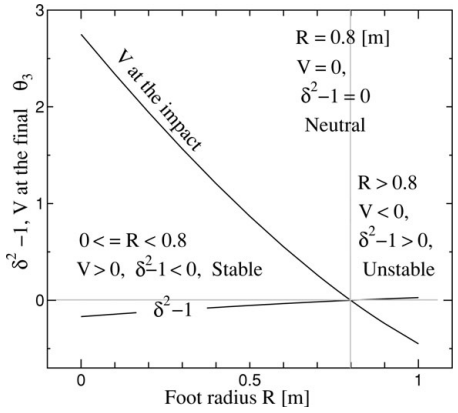

Fig. 9. The property of stability with respect to the foot radii R. Two black solid lines show V and $\delta^2 - 1$. V and $\delta^2 - 1$ have opposite sign thus a cyclic motion may exist such that (45) is satisfied. For $R < 0.8$ m the motion is stable. For $R > 0.8$ m the motion is unstable. For $R = 0.8$ m the motion is neutral, that is all of ξ_c are cyclic motions.

https://doi.org/10.1017/S0263574708005006 Published online by Cambridge University Press

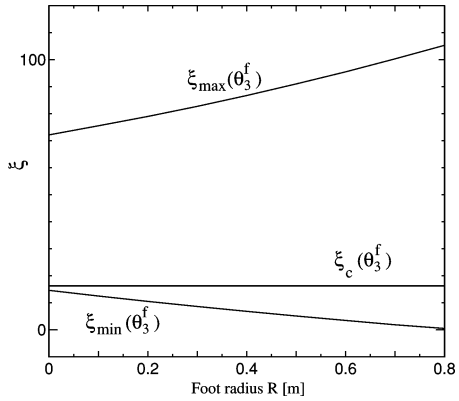

Fig. 10. Basin of attraction of ξ w.r.t. the foot radii R. The area between the line of $\xi_{\min}(\theta_3^f)$ and $\xi_{\max}(\theta_3^f)$ is the basin of attraction by the numerical method. The line ξ_c means the cyclic motions. In the upper area of $\xi_{\max}(\theta_3^f)$, vertical reaction forces are negative. There would be a flight phase. In the lower area of $\xi_{\min}(\theta_3^f)$, the velocity of the monotonic variable after the impact is not large enough to produce a step, $\xi_{\min}(\theta_3^f)$ is given by (45). After the beginning of the step, the biped goes backward or stands still eventually.

finds results that are different from our results. For passive walking he finds that from the stability point of view the best radius is 14% of leg length, this value corresponds to a case where two monotonic lines of eigenvalues are crossing. The increasing one is represented "Speed mode," and the decreasing one is "Totter mode." However the crossing point changes with respect to slope angle and physical parameters of bipeds. The 14% of leg length is not the best radius, generally speaking. In our controlled system, it is predictable that the "Totter mode" is close to zero or much smaller than the "Speed mode," since the "Speed mode" is expressed by the zero dynamics of the controlled system and the 'Totter mode' is depending on the controller gains. Term δ^2 has the same property of the "Speed mode," and thus is increasing with respect to R. In our case we are not interested in the best solution but in the limit where stability exists, thus there are no contradiction with the results of Wisse[16].

6.3. Basin of attraction

Basins of attraction determined by numerical computations are shown in Fig. 10. The basin is expressed by pseudo-kinetic energy because we assume that the output h converges to the reference path. The larger the foot radii are in the stable domain, the wider the basin of attraction is but the slower the speed of convergence is. If the foot radius is the same as the leg length, the motion is neutral, that is, all motions are cyclic.

In Fig. 10, the area between the line of $\xi_{\min}^-$ and $\xi_{\max}^-$ is the basin of attraction. The variable ξ just before the impact is used for expressing the basin of attraction. The line ξ_c represents the cyclic motions. Figure 11 presents time evolutions of θ_3, $\dot{\theta}_3$ for 100 steps. The following foot radii are considered: $R = 0$ m, 0.5 m , 0.8 m, and 1.3 m. The first two cases are clearly stable, the case, $R = 0.8$ m, is neutral, and the case, $R = 1.3$ m, is unstable. Simulations confirm the existence of the neutral condition.

The property of the basin of attraction with respect to the radius is also analogous to the results of passive dynamic walking by Wisse.[14] As depicted in Fig. 10, the bottom

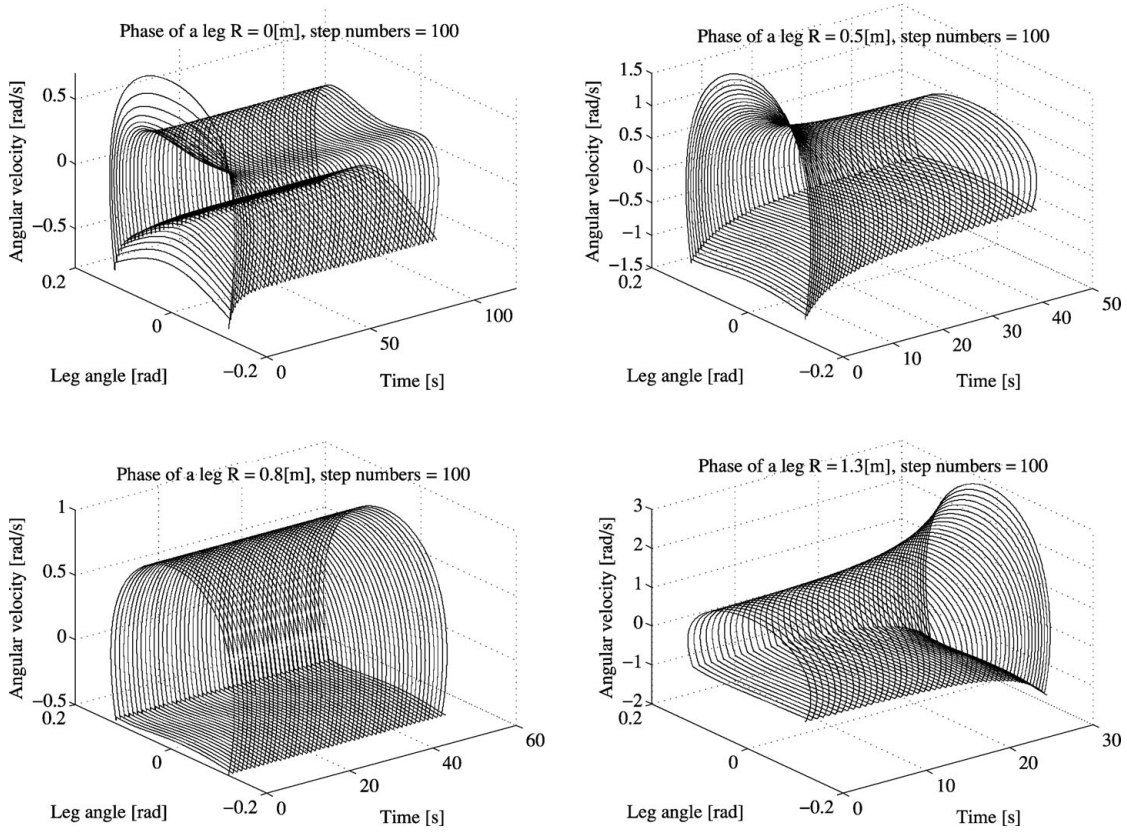

Fig. 11. Time evolutions of phases for the first leg at the foot radii $R = 0$ m (stable), 0.5 m (stable), 0.8 m (neutral), and 1.3 m (unstable).

https://doi.org/10.1017/S0263574708005006 Published online by Cambridge University Press

line shows minimal ξ corresponding to $\xi_{\min}$. It means a required minimal angular momentum to overcome a gap from a minimum of a vertical position of CoM to a maximum. If the momentum is smaller than the minimum, the complete step is not achieved, the step begins and then the robot goes backward to return to its initial configuration for the step. After that, the robot stops, but it does not fall down contrarily to a passive dynamic walker[15] that falls down backward.

From Fig. 5, the smaller the radius is, the larger the gaps of the vertical positions of CoM and the minimal ξ^-_{min} are. Thus the circular arc feet broaden the minimal bounds. The variation of the maximal bounds is caused by the limits on the vertical reaction forces to avoid taking off. The reaction force vector R_1 at the point N_1 is given by the following equation:

$$R_1 = \begin{bmatrix} R_{x_1} \\ R_{y_1} \end{bmatrix} = \begin{bmatrix} M\ddot{x}_G \\ M(\ddot{y}_G + g) \end{bmatrix}. \tag{60}$$

The vertical acceleration $\ddot{y}_G$ is decided by the centrifugal force caused by the angular velocity of the stance leg $\dot{\theta}_3$ and an acceleration of the leg variation $\ddot{l}_i(t)$. The radius smoothens the variation of CoM, and consequently the centrifugal force is reduced. We observe that the acceleration of the leg is smaller when the radii increase. Thus, the maximal ξ^-_{max} is extended when the radius increases. Namely, the basin of attraction is broaden by the physical properties such as the feet radii. Globally, our controlled system has similar properties for stability and basin of attraction to the passive dynamic walking.

6.4. *Consumed energy*

Consumed energies for one cyclic step with respect to the foot radii R is described in Fig. 12. The following formula is used for computing the consumed energy:

$$E_c = \int_0^T |\dot{\theta}' \cdot B \cdot \Gamma| dt. \tag{61}$$

The larger the foot radius is, the smaller the consumed energy is for the cyclic motion, even if the motion becomes unstable. Thus, the circular arc feet are effective in reducing the consumed energy.

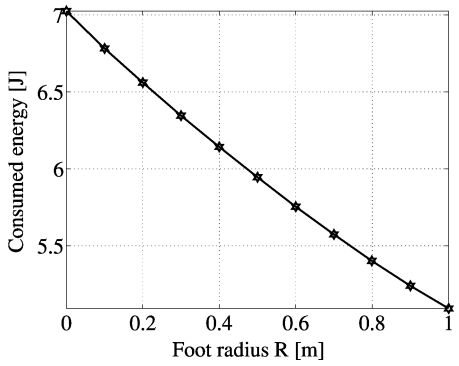

Fig. 12. Consumed energy for one cyclic step w.r.t. the foot radii R by the numerical simulation. The torso angle is chosen so that $\xi = 16.27$ by the analytic solution for all R.

6.5. *Optimal radius*

There is a trade-off property between the convergence speed, the basin of attraction, and the energy consumption. What we can say is that nearer the radius is to the leg length, the slower the speed of convergence is and the larger the basin is. "Foot clearance problem" does not appear because of the variable length legs in our case. In the cases of "Anthropomorphic Model" and "Simplest Model" of Adamczyk's result,[19] the CoM mechanical work property with respect to feet radii is similar to our result of consumed energy. However, in their cases of "Forward-foot Model" and "Kneed Model," the work had a minimum.

The suggestion of McGeer's to choose a foot radius of 1/3 of leg lengths can also be considered in our discussion. It might be better to choose a larger radius (e.g., between a half and three quarters) to have a large basin of attraction even if the speed of convergence is slower.

6.6. *Unstable walking with radii greater than the leg length*

Kuo's analysis 21 of the CoM velocity contradicts our study because he considers a simple model with rigid legs and circular arc feet and the CoM is located at hip position, and we consider prismatic knees. The right of Fig. 5 presents the evolution of the CoM relative to the simple model.[21] Tangent vectors of right ends of lines are expressing the pre-impact velocity of CoM, and tangent vectors of left ends of lines are expressing the post-impact velocity of CoM. When R $>$ 0.8 m, the change of CoM velocities are upward, which means the impulsive force at the impact is negative. It actually would be a flight phase. Left part of Fig. 5 gives the CoM evolution in the case of our biped shown in Fig. 2. Since all of the ranges of velocities of CoM at the impact are downward, it never fails to flight phase for any radius. In fact, our biped has prismatic knees and CoM is mainly distributed on the torso which is swinging a little. A lot of paths can be chosen for the CoM position differently from the simple model.

7. Conclusion

In the paper, some effects of circular arc feet for a planar biped via a geometric tracking were taken into account. An analytic solution of Poincaré map was given for the controlled system. Stability of walking was analyzed by the Poincaré map and the following results are obtained:

- Radius of the circular arc feet affects the stability of walking, and the speed of convergence decreases when the radius approaches to a leg length.
- A basin of attraction is broadened by choosing larger radii and the controller can stabilize the biped walking in the largest basin of attraction for the radii less than the leg length.

The leg length and the radius smoothen the variation and reduce the impact velocity. From the properties of the reference paths, the radius of the foot has a significant effect for the stability and the basin of attraction. The results are analogous to those[8,14] and the prospect[15] on passive dynamic walking. The geometric tracking method does not change the general effect of the circular arc feet. A reduction of the vertical CoM variation by the foot radius is functional not

https://doi.org/10.1017/S0263574708005006 Published online by Cambridge University Press

only for the geometric tracking method but for general biped walking. However the motion of CoM and the consumed energy are different from some very simple models because our model has variable length of legs and a torso.

References

1. Y. Aoustin and A. M. Formal'sky, "Design of Reference Trajectory to Stabilize Desired Nominal Cyclic Gait of a Biped," *Proceedings of the International Workshop on Robot Motion and Control*, ROMOCO'99, (1999) pp. 159–165.
2. J. Grizzle, G. Abba and F. Plestan, "Asymptotically stable walking for biped robots: Analysis via systems with impulse effects," *IEEE Trans. Automat. Contr.* **46**(1), 51–64 (2001).
3. Y. Aoustin and A. M. Formal'sky, "Control design for a biped reference trajectory based on driven angles as functions of the undriven Angle," *J. Comput. Syst. Sci. Int.* **42**(4), 159–176 (2003).
4. C. Chevallereau, G. Abba, Y. Aoustin, F. Plestan, E. R. Westervelt, C. Canudas-De-Wit and J. W. Grizzle, "Rabbit: A test bed for advanced control theory," *IEEE Contr. Syst. Mag.* **23**(5), 57–79 (Oct. 2003).
5. J. Furusho, H. Moritsuka and M. Masubuchi, "Low order modeling of biped locomotion system using local feedback," *Trans. Soc. Instrum. Contr. Eng.* **17**(5), 596–601, (1981) in Japanese.
6. S. Kajita and K. Tani, "Study of Dynamic Biped Locomotion on Rugged Terrain – Derivation and Application of the Linear Inverted Pendulum Mode," *Proceedings of IEEE International Conference on Robotics and Automation* (1991) pp. 1405–1411.
7. E. R. Westervelt, G. Buche and J. W. Grizzle, "Experimental validation of a framework for the design of controllers that induce stable walking in planar bipeds," *Int. J. Robot. Res.* **24**(6), 559–582 (2004).
8. T. McGeer, "Passive dynamic walking," *Int. J. Robot. Res.* **9**, 62–82 (1990).
9. T. Kinugasa, Y. Hashimoto and H. Fushimi, "Passive Walking of Biped Emu with Attitude Control of Body," *Proceedings of IEEE/RSJ International Conference on Intelligent Robots and Systems* (2003) pp. 346–359.
10. T. Kinugasa, K. Osuka and S. Miwa, "Biped walking by variations of knee lengths and attitude control of a body and its frequency Analysis," *J. Robot. Soc. Japan* **25**(3), (2007) in Japanese.
11. T. Kinugasa, S. Miwa and K. Yoshida, "Frequency analysis for biped walking via length variation of legs," *J. Robot. Mech.* **20**(1), 98–105 (2008).
12. C. Chevallereau and D. Djoudi, "Feet can Improve the Stability Property of a Control Law for a Walking Robot," *Proceedings of International Conference on Robotics and Automation*, (2006) pp. 1206–1212.
13. C. Chevallereau, D. Djoudi and J. W. Grizzle, "Stable bipedal walking with foot rotation through direct regulation of the zero moment point," *IEEE Trans. Robot.* **24**(2), 390–401 (2008).
14. M. Wisse and J. van Frankenhuyzen, "Design and Construction of Mike; A 2D Autonomous Biped based on Passive Dynamic Walking," *Proceedings of Conference on Adaptive Motion of Animals and Machines WeP-I-1*, Springer, Tokyo (2003).
15. M. Wisse, A. L. Schwab, R. Q. van der Linde and F. C. T. van der Helm, "How to keep from falling forward: Elementary swing leg action for passive dynamic walkers," *IEEE Trans. Robot.* **21**(3), 393–401 (2005).
16. M. Wisse, D. G. E. Hobbelen, R. J. J. Rotteveel, S. O. Anderson and G. J. Zeglin, "Ankle Springs Instead of Arc-shaped Feet for Passive Dynamic Walkers," *Proceedings of Humanoids 2006*, (2006) pp. 110–116.
17. F. Asano and Z. W Luo, "On Energy-Efficient and High-Speed Dynamic Biped Locomotion with Semicircular Feet," *Proceedings of the 2006 IEEE/RSJ International Conference on Intelligent Robots and Systems*, (2006) pp. 5901–5906.
18. F. Asano and Z. W. Luo, "The Effect of Semicircular Feet on Energy Dissipation by Heel-strike in Dynamic Biped Locomotion," *Proceedings of IEEE International Conference on Robotics and Automation*, (2007) pp. 3976–3981.
19. P. G. Adamczyk, S. H. Collins and A. D. Kuo, "The advantages of a rolling foot in human walking," *J. Exp. Biol.* **209**, 3953–3963 (2006).
20. B. Morris and J. W. Grizzle, "A Restricted Poincare Map for Determining Exponentially Stable Periodic Orbits in Systems with Impulse Effects: Application to Bipedal Robots," *Proceedings of IEEE Conference on Decision and Control*, (2005) pp. 4199–4206.
21. A. D. Kuo, "Energetics of actively powered locomotion using the simplest walking model," *J. Biomech. Eng.* **124**, 113–120 (2001).
22. C. Chevallereau, A. Formal'sky and D. Djoudi, "Tracking of a joint path for the walking of an underactuated biped," *Robotica* **22**, 15–28, (2004).

https://doi.org/10.1017/S0263574708005006 Published online by Cambridge University Press